INTECH
open science | open minds

OPEN ACCESS
ARTICLE

International Journal of Advanced Robotic Systems

Kinematically Redundant Parallel Haptic Device with Large Workspace

Regular Paper

Han Sung Kim[1,*]

1 Department of Mechanical Engineering, Kyungnam University, Korea
* Corresponding author E-mail: hkim@kyungnam.ac.kr

Received 9 May 2012; Accepted 11 Sep 2012

DOI: 10.5772/53279

Abstract In this paper, a kinematically redundant parallel haptic device with large workspace is presented. The haptic device has a similar kinematic structure to the well-known Delta manipulator. However, it has a special arrangement of actuators and one redundant actuator added to the third leg. The proposed haptic device has essentially 4-DOF, however, only three translational DOF are used for 3-DOF positioning and force reflection, and one rotational DOF by the redundant actuator is used to increase well-conditioned workspace. If the redundant actuator's angle is controlled to follow x and y position, the haptic device has a large cylindrical workspace and can maintain good kinematic and statics performance over the whole workspace. The kinematics and workspace are analysed, and the optimal design method of finding minimum link lengths to satisfy prescribed workspace is presented. Finally, the prototype haptic device and control experiment result are presented.

Keywords Haptic Device, Kinematic Redundancy, Delta Parallel Manipulator, Optimal Design, Workspace Analysis

1. Introduction

Haptic devices have been extensively investigated and applied to many fields, such as teleoperation, robotic surgery, bioengineering, computer-aided design, etc. In order to provide realistic force reflection and high manipulability to an operator, the mechanism of a haptic device should have low inertia, high stiffness, large force reflection capability, good kinematic conditioning, as well as large workspace, back-drivability, low friction and small moving inertia.

In general, serial-kinematic haptic devices [1-8] have large workspace, but relatively small force reflection and low stiffness. In order to further increase force reflection and stiffness, parallel-kinematic manipulators have been employed as haptic device mechanisms [9-14]. One of the most famous parallel-type haptic devices may be Delta haptics [15-18]. The Delta parallel manipulator has large force reflection and high stiffness due to parallel structure and parallelogram. However, it has a smaller workspace compared to the serial one. A new parallel manipulator similar to Delta called "Tau" with a large cylindrical workspace as with a SCARA robot is also presented [19-21]. However, the Tau manipulator consists of three different leg configurations and the kinematic performance is not symmetric. Comprehensive reviews of the mechanisms of haptic devices can be found in [22, 23]. In general, redundancy can improve the workspace and performance of a parallel manipulator [24, 25]. By adding

more than one active joint to a non-redundant parallel manipulator, a kinematically redundant parallel manipulator can be constructed.

In this paper, a kinematically redundant parallel manipulator for a haptic device is conceived, which retains the advantages of both serial (large workspace) and parallel (large force and high stiffness) manipulators. The proposed parallel manipulator has the special arrangement of actuators and one redundant actuator for large workspace and good performance. The position, Jacobian and workspace analyses are performed. The optimal design to find minimum link lengths satisfying the prescribed workspace is presented. Finally, a numerical example of the optimal design, prototype haptic device and control experiment result are presented.

2. Position Analysis

As shown in Fig. 1, the kinematic structure of the proposed haptic device is similar to that of the well-known Delta manipulator with three *R*-*Pa* (Revolute-spatial Parallelogram) legs [15]. However, the moving platform of the proposed haptic device is connected to the fixed base by two *R*-*Pa* legs on the horizontal plane and one *R*-*R*-*Pa* leg on the vertical plane, where *R* denotes an actuated revolute joint. Specifically, the axes of the first and second rotary actuators (R_1 and R_2) are placed along the z-axis and the axis of the third rotary actuator (R_3) is perpendicular to the z-axis. One redundant actuator (R_4) rotates the third rotary actuator and leg about the z-axis together with the angle of α. This parallel haptic device has 4-DOF, i.e., three translations and one rotation about the z-axis (α). It is clear that the angle of the moving platform is equal to that of the redundant actuator's angle (α) due to the parallelogram of $l_{3,2}$.

If the redundant actuator is controlled to follow input x and y position, i.e., $\alpha = \text{Atan2}(p_y, p_x)$, the connecting link of the third leg ($l_{3,2}$) can be kept vertically and then $\theta_{3,3} = 0$. With this control method, the workspace is not limited by the range of $\theta_{3,3}$ and the manipulator can maintain better kinematic and statics performance over the whole workspace than that of $\theta_{3,3} \neq 0$ (refer to Fig. 3). The parallel haptic device can be treated as a 3-DOF positioning one. The first two actuators determine the x and y positions of the moving platform, and the third actuator controls the z position. If the first two actuators and the redundant actuator can make a complete circle around the z-axis, the whole workspace becomes a large hollow cylinder.

As shown in Fig. 1, the global reference frame is attached to the fixed base at O, and the ith local frame is attached at point A_i. It is noted that the frames A_1 and A_2 coincide with the reference frame.

For each leg, the following vector-loop equation should be satisfied [28].

$$\overline{A_iM_i} + \overline{M_iB_i} = \overline{OP} + \overline{PB_i} - \overline{OA_i} \text{ for } i = 1,2,3 \qquad (1)$$

Expressing Eq. (1) with respect to each local frame A_i yields

$$l_{i,1}\,{}^i\mathbf{u}_{i,1} + l_{i,2}\,{}^i\mathbf{u}_{i,2} = {}^i\mathbf{b}_i \qquad (2)$$

where ${}^i\mathbf{v}_{i,j}$ is the jth vector in the ith leg expressed in frame A_i and $s_{i,j}$ is the jth scalar quantity in the ith leg in this paper. The unit directional vectors of links are given by

$${}^i\mathbf{u}_{i,1} = \begin{bmatrix} c\theta_{i,1} \\ s\theta_{i,1} \\ 0 \end{bmatrix}, \text{ and } {}^i\mathbf{u}_{i,2} = \begin{bmatrix} c\theta_{i,12}c\theta_{i,3} \\ s\theta_{i,12}c\theta_{i,3} \\ s\theta_{i,3} \end{bmatrix}. \qquad (3)$$

where $\theta_{i,12} = \theta_{i,1} + \theta_{i,2}$. The position vector of $\overline{A_iB_i}$ expressed in frame A_i, ${}^i\mathbf{b}_i = [b_{i,x}, b_{i,y}, b_{i,z}]^T$, is obtained by

$${}^1\mathbf{b}_1 = \begin{bmatrix} p_x \\ p_y \\ p_z \end{bmatrix} + \begin{bmatrix} bs\alpha \\ -bc\alpha \\ 0 \end{bmatrix}, \; {}^2\mathbf{b}_2 = \begin{bmatrix} p_x \\ p_y \\ p_z \end{bmatrix} + \begin{bmatrix} -bs\alpha \\ bc\alpha \\ 0 \end{bmatrix},$$

$${}^3\mathbf{b}_3 = \begin{bmatrix} c\alpha & s\alpha & 0 \\ 0 & 0 & -1 \\ -s\alpha & c\alpha & 0 \end{bmatrix} \begin{bmatrix} p_x \\ p_y \\ p_z \end{bmatrix} + \begin{bmatrix} 0 \\ a-b \\ 0 \end{bmatrix}. \qquad (4)$$

In the following analyses, it is assumed that the redundant actuator's angle α is given and the 4-DOF parallel manipulator will be considered as a 3-DOF positioning one. The inverse position analysis can be defined as the problem of finding the joint angle vector, $\mathbf{q} = [\theta_{1,1}, \theta_{2,1}, \theta_{3,1}]^T$ for given the end-effector position vector, $\mathbf{x} = [p_x, p_y, p_z]^T$. First, $\theta_{3,i}$ can be calculated from the third element of Eq. (2) as

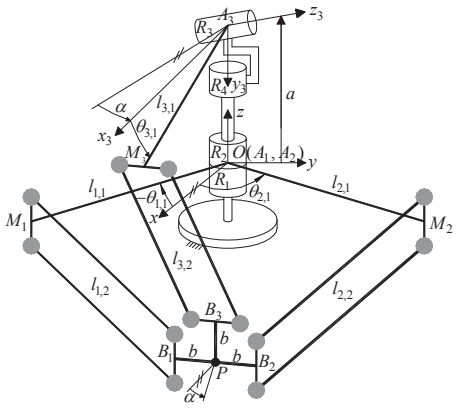

Figure 1. Kinematic structure of a Delta-like parallel haptic device.

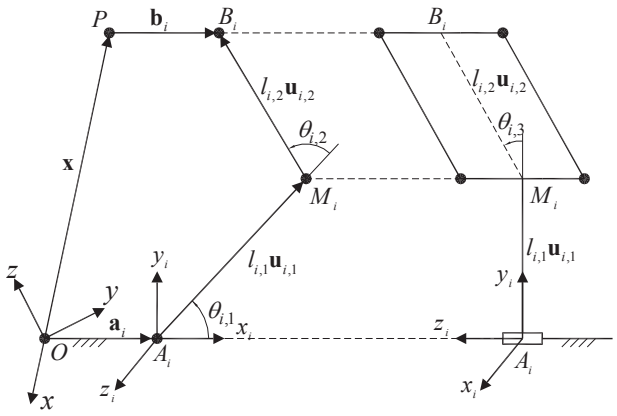

Figure 2. Description of the joint angles in the *i*th leg.

$$\theta_{i,3} = \sin^{-1}\frac{b_{i,z}}{l_{i,2}}. \tag{5}$$

By summing the squares of $b_{i,x}$, $b_{i,y}$, and $b_{i,z}$ in Eq. (2), an equation with only $\theta_{i,2}$ can be obtained.

$$2l_{i,1}l_{i,2}c\theta_{i,3}c\theta_{i,2} + l_{i,1}^2 + l_{i,2}^2 = b_{i,x}^2 + b_{i,y}^2 + b_{i,z}^2 \tag{6}$$

Solving Eq. (6) for $\theta_{i,2}$ results in

$$\theta_{i,2} = \cos^{-1}\lambda \tag{7}$$

where $\lambda = (b_{i,x}^2 + b_{i,y}^2 + b_{i,z}^2 - l_{i,1}^2 - l_{i,2}^2)/(2l_{i,1}l_{i,2}c\theta_{i,3})$. Once $\theta_{i,3}$ and $\theta_{i,2}$ are determined, $\theta_{i,1}$ can be obtained from Eq. (2).

$$\theta_{i,1} = \text{Atan2}(-g_{i,2}b_{i,x} + g_{i,1}b_{i,y}, g_{i,1}b_{i,x} + g_{i,2}b_{i,y}) \tag{8}$$

where $g_{i,1} \equiv l_{i,1} + l_{i,2}c\theta_{i,2}c\theta_{i,3}$ and $g_{i,2} \equiv l_{i,2}s\theta_{i,2}c\theta_{i,3}$. It is noted that if $|b_{i,z}| > l_{i,2}$ or $|\kappa| > 1$, the given position is out of the workspace.

The problem of the forward position analysis is to find end-effector position $\mathbf{x}$ for the given joint angle vector $\mathbf{q}$. Rewriting Eq. (2) yields

$$l_{i,2}\,{}^i\mathbf{u}_{i,2} = {}^i\mathbf{b}_i - l_{i,1}\,{}^i\mathbf{u}_{i,1}. \tag{2'}$$

By summing the squares of the three components of Eq. (2′), the following sphere equation for the *i*th leg is obtained by

$$l_{i,2}^2 = b_{i,x}^2 + b_{i,y}^2 + b_{i,z}^2 + l_{i,1}^2 - 2l_{i,1}c\theta_{i,1}b_{i,x} - 2l_{i,1}s\theta_{i,1}b_{i,y}. \tag{9}$$

The plane equation that contains the circle of intersection made by the spheres of leg 3 and leg *j* is determined by subtracting Eq. (9) for $i = j$ from Eq. (9) for $i = 3$:

$$e_{j,1}p_x + e_{j,2}p_y + e_{j,3}p_z + e_{j,4} = 0 \quad \text{for } j = 1,2 \tag{10}$$

where

$$e_{j,1} = 2(l_{j,1}c\theta_{j,1} - l_{3,1}c\alpha c\theta_{3,1} + (-1)^j bs\alpha),$$

$$e_{j,2} = 2(l_{j,1}s\theta_{j,1} - l_{3,1}s\alpha c\theta_{3,1} - (-1)^j bc\alpha),$$

$$e_{j,3} = 2(-a + b + l_{3,1}s\theta_{3,1}),$$

$$e_{j,4} = 2\{(-1)^j bl_{j,1}(c\alpha s\theta_{j,1} - s\alpha c\theta_{j,1}) + l_{3,1}s\theta_{3,1}(b-a)\} + a^2 - 2ab - l_{j,1}^2 + l_{3,1}^2 + l_{j,2}^2 - l_{3,2}^2$$

Solving Eq. (10) for p_x and p_y in terms of p_z and then substituting the resulting expressions into Eq. (9) for $i = 3$ yields

$$k_0 p_z^2 + k_1 p_z + k_2 = 0 \tag{11}$$

where

$$k_0 = 1 + (q_1^2 + q_4^2)/q_2^2,$$

$$k_1 = 2(q_0q_1 + q_3q_4)/q_2^2 - 2l_{3,1}c\theta_{3,1}(q_1c\alpha + q_4s\alpha)/q_2 + 2(l_{3,1}s\theta_{3,1} - a + b),$$

$$k_2 = (q_0^2 + q_3^2)/q_2^2 - 2l_{3,1}c\theta_{3,1}(q_0c\alpha + q_3s\alpha)/q_2 - 2l_{3,1}s\theta_{3,1}(a-b) + (l_{3,1}^2 - l_{3,2}^2) + (a-b)^2,$$

$$q_0 = e_{1,2}e_{2,4} - e_{2,2}e_{1,4},\ q_1 = e_{1,2}e_{2,3} - e_{2,2}e_{1,3},$$

$$q_2 = e_{1,1}e_{2,2} - e_{1,2}e_{2,1},\ q_3 = e_{2,1}e_{1,4} - e_{1,1}e_{2,4},$$

$$q_5 = e_{2,1}e_{1,3} - e_{1,1}e_{2,3}.$$

Once p_z is found, p_x and p_y can be determined by back substitution into Eq. (10).

3. Jacobian analysis

Differentiating Eq. (2) with respect to time yields

$${}^i\dot{\mathbf{x}} = l_{i,1}({}^i\boldsymbol{\omega}_{i,1} \times {}^i\mathbf{u}_{i,1}) + l_{i,2}({}^i\boldsymbol{\omega}_{i,2} \times {}^i\mathbf{u}_{i,2}) \quad \text{for } i = 1,2,3 \tag{12}$$

where ${}^i\dot{\mathbf{x}}$ is the linear velocity of the moving platform and ${}^i\boldsymbol{\omega}_{i,j}$ is angular velocity of the *j*th link of the *i*th leg with respect to frame A_i. To eliminate the passive joint rate, dot-multiplying both sides of Eq. (12) by ${}^i\mathbf{u}_{i,2}$ yields

$${}^i\mathbf{u}_{i,2} \cdot {}^i\dot{\mathbf{x}} = l_{i,1}\,{}^i\boldsymbol{\omega}_{i,1} \cdot ({}^i\mathbf{u}_{i,1} \times {}^i\mathbf{u}_{i,2}). \tag{13}$$

Expressing the vectors in Eq. (13) in frame A_i gives

$${}^i\boldsymbol{\omega}_{i,1} = \begin{bmatrix} 0 \\ 0 \\ \dot{\theta}_{i,1} \end{bmatrix} \text{ for } i = 1,2,3,$$

$$ {}^1\dot{\mathbf{x}} = {}^2\dot{\mathbf{x}} = \begin{bmatrix} \dot{p}_x \\ \dot{p}_y \\ \dot{p}_z \end{bmatrix}, \quad {}^3\dot{\mathbf{x}} = \begin{bmatrix} c\alpha & s\alpha & 0 \\ 0 & 0 & -1 \\ -s\alpha & c\alpha & 0 \end{bmatrix} \begin{bmatrix} \dot{p}_x \\ \dot{p}_y \\ \dot{p}_z \end{bmatrix} \tag{14} $$

and ${}^i\mathbf{u}_{i,2}$ is given in Eq. (3). Writing Eq. (13) three times, once for each for i=1, 2, and 3, yields three scalar equations, which can be assembled in matrix form as

$$ J_x^T \dot{\mathbf{x}} = J_q \dot{\mathbf{q}} \tag{15} $$

where $\dot{\mathbf{q}} = [\dot{\theta}_{1,1}, \dot{\theta}_{2,1}, \dot{\theta}_{3,1}]^T$,

$$ J_x = \begin{bmatrix} c\theta_{1,12}c\theta_{1,3} & c\theta_{2,12}c\theta_{2,3} & c\theta_{3,12}c\theta_{3,3}c\alpha - s\theta_{3,3}s\alpha \\ s\theta_{1,12}c\theta_{1,3} & s\theta_{2,12}c\theta_{2,3} & c\theta_{3,12}c\theta_{3,3}s\alpha + s\theta_{3,3}c\alpha \\ s\theta_{1,3} & s\theta_{2,3} & -s\theta_{3,12}c\theta_{3,3} \end{bmatrix}, $$

$$ J_q = \begin{bmatrix} l_{1,1}s\theta_{1,2}c\theta_{1,3} & 0 & 0 \\ 0 & l_{2,1}s\theta_{2,2}c\theta_{2,3} & 0 \\ 0 & 0 & l_{3,1}s\theta_{3,2}c\theta_{3,3} \end{bmatrix}. \tag{16} $$

If J_q is not singular, Eq. (15) can be rewritten by

$$ \dot{\mathbf{q}} = J^T \dot{\mathbf{x}} \tag{17} $$

where $J = J_x J_q^{-1}$.

Using the principle of virtual work, the statics relation is obtained by

$$ \mathbf{F} = J\,\boldsymbol{\tau} \tag{18} $$

where $\mathbf{F} = [f_x, f_y, f_z]^T$ and $\boldsymbol{\tau} = [\tau_1, \tau_2, \tau_3]^T$ denote the end-effector force and joint torque vectors, respectively.

The stiffness mapping in the joint space can be expressed by

$$ \boldsymbol{\tau} = [k]\delta\mathbf{q} \tag{19} $$

where $[k] = \mathrm{diag}(k_1, k_2, k_3)$ denotes a 3×3 diagonal matrix representing the joint stiffness. Applying the velocity and statics relations to Eq. (19), the stiffness mapping in the Cartesian space can be expressed by

$$ \mathbf{F} = K\delta\mathbf{x} \tag{20} $$

where $\delta\mathbf{x} = [\delta p_x, \delta p_y, \delta p_z]^T$ and the stiffness matrix is given by

$$ K = J[k]J^T. \tag{21} $$

4. Workspace analysis and optimal design

If the redundant actuator is controlled simply with $\alpha = \tan^{-1}(p_y / p_x)$, the kinematically redundant parallel haptic device can have a large well-conditioned workspace. Furthermore, using the control method, the design problem can be reduced to a planar one. In other words, this manipulator is symmetric at every $x'z$ plane with the incident angle of α to the xz plane. The optimal design will be performed on the $x'z$ plane.

Figures 3(a) and 3(b) demonstrate that the kinematic and statics performances (isotropy condition [26] and minimum force transmission capability [27]) when using this control method are larger than those when using a fixed angle, $\alpha = 0$, which is the case for a non-redundant manipulator such as the typical Delta. The isotropy condition and minimum force transmission capability are defined by

$$ \kappa = 1/\mathrm{cond}(J), \quad \sigma_{\min} = \sqrt{\min(\mathrm{eig}(JJ^T))}. \tag{22} $$

First, the minimum length of b can be selected to prevent the interference of parallelograms. The length of b is dependent on the width of a parallelogram. It is noted that a smaller length of (a – b) is desirable for smaller link lengths of leg 3 (refer to Fig. 5 and Eq. (30b)). In the prototype development, a=85 and b=35 [mm] are chosen.

Once [a, b] are determined, the objective of the optimal design can be defined as a problem to determine a set of minimum link lengths to satisfy the prescribed work area. The kinematic design variables of the optimal design are selected as

$$ [l_{p1}, l_{p2}, l_{z1}, l_{z2}] \tag{23} $$

where $l_{p1} \equiv l_{1,1} = l_{2,1}$, $l_{p2} \equiv l_{1,2} = l_{2,2}$, $l_{z1} \equiv l_{3,1}$ and $l_{z2} \equiv l_{3,2}$.

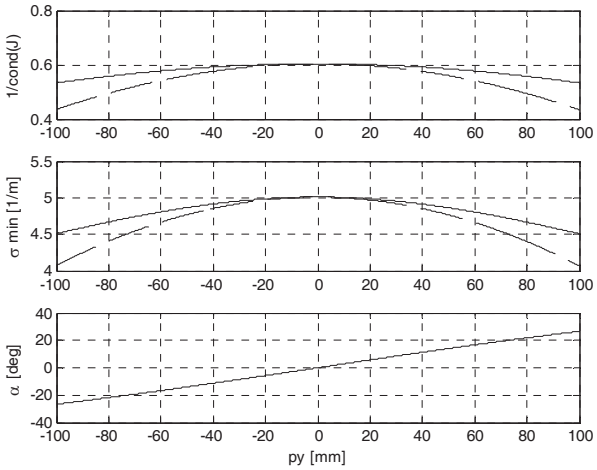

Figure 3. (a). Along the y-axis (x=200, z=0 [mm])

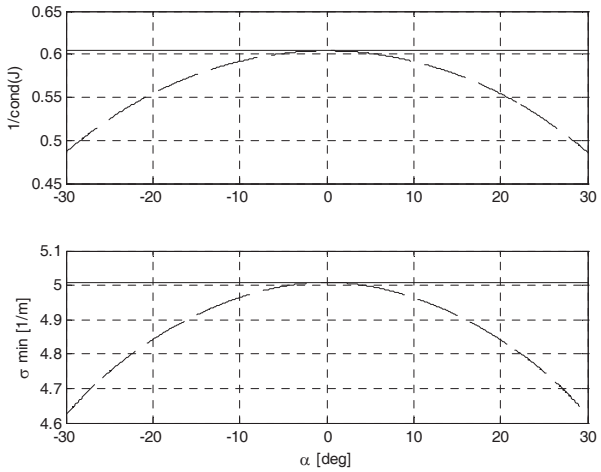

Figure 3. (b). For circular path (x=200cos(α), y=200sin(α), z=0 [mm]) (dotted line: $\alpha = 0$, solid line: $\alpha = \tan^{-1}(p_y / p_x)$)

The prescribed work area on the $x'z$ plane is defined as a rectangle.

$$A_p = w \times h \tag{24}$$

The angular limits of the passive joints are chosen by

$$\beta_{\min} < |\theta_{i,2}| < \beta_{\max}, \ |\theta_{i,3}| < \gamma_{\max} \text{ for } i = 1,2,3 \tag{25}$$

where the angular limit of the second passive joint is introduced to prevent serial singular configuration and that of the third passive joint comes from a spherical joint limit.

First, the height of the work area is limited by the second link lengths and the third joint angle limits of the first and second legs as

$$l_{p2} = \frac{h}{2\sin\gamma_{\max}}. \tag{26}$$

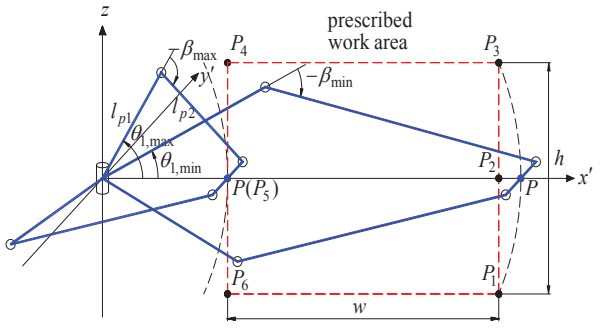

Figure 4. Work area limited by legs 1 and 2.

The next step is to determine l_{p1} by considering the minimum and maximum configurations of the first and second legs. For simplicity of expression, the leg number is omitted. As shown in Fig. 4, the $x_{\min}$ of the end-effector should be smaller than P_5.

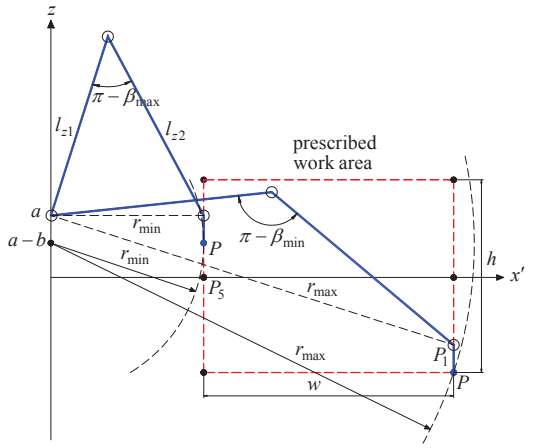

Figure 5. Work area limited by leg 3.

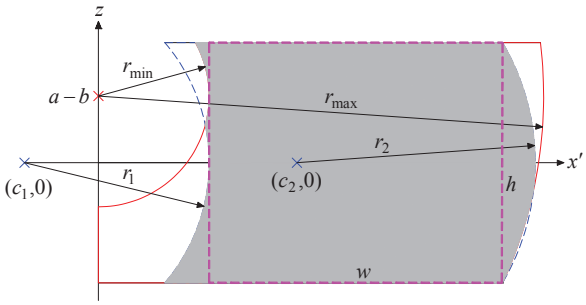

Figure 6. Workspace plot on the $x'z$ plane.

$$x_{\min} = l_{p1}\cos\theta_{1,\max} + l_{p2}\cos(\theta_{1,\max} - \beta_{\max}) \tag{27a}$$

$$l_{p1}\sin\theta_{1,\max} + l_{p2}\sin(\theta_{1,\max} - \beta_{\max}) = b \tag{27b}$$

As shown in Fig. 5, the $x_{\max}$ of the end-effector should be larger than P_1 or P_3.

$$x_{\max} = l_{p1}\cos\theta_{1,\min} + l_{p2}\cos(\theta_{1,\min} - \beta_{\min})\cos\gamma_{\max} \tag{28a}$$

$$l_{p1}\sin\theta_{1,\min} + l_{p2}\sin(\theta_{1,\min} - \beta_{\min})\cos\gamma_{\max} = b \tag{28b}$$

The minimum length of the arms (l_{p1}) of the first and second legs can be determined by

$$x_{\max}(l_{p1}) - x_{\min}(l_{p1}) \geq w \tag{29}$$

The numerical iteration method is used to determine l_{p1}. First, $\theta_{1,\max}$ and $\theta_{1,\min}$ are solved by using Eqs. (27b) and (28b) with assumed l_{p1}, and $x_{\min}$ and $x_{\max}$ are calculated by Eqs. (27a) and (28a). If the condition of Eq. (29) is not satisfied, the first step is repeated with a new l_{p1}.

Finally, l_{z1} and l_{z2} are determined by the intersection area of following inequality conditions.

$$r_{\min}^2 = l_{z1}^2 + l_{z2}^2 + 2l_{z1}l_{z2}\cos\beta_{\max} \leq x_{\min}^2 \tag{30a}$$

$$r_{\max}^2 = l_{z1}^2 + l_{z2}^2 + 2l_{z1}l_{z2}\cos\beta_{\min} \geq x_{\max}^2 + (a - b + h/2)^2 \tag{30b}$$

In general, the work area including the prescribed one is determined by the intersection area of the four circles and $-h/2 \le z \le h/2$. In Fig. 6, the centres and radii related to the first and second legs are given by

$$c_1 = l_{p1}\cos\theta_{1,\max},\ r_1 = l_{p2}\cos(\theta_{1,\max} - \beta_{\max}),$$

$$c_2 = l_{p1}\cos\theta_{1,\min},\ r_2 = l_{p2}\cos(\theta_{1,\min} - \beta_{\min}). \quad (31)$$

5. Prototype development and control experiment

In the prototype design, the prescribed work area and other kinematic parameters are selected as

$$A_p = w \times h = 220 \times 180\ [\text{mm}^2],\ a = 85,\ b = 35\ [\text{mm}].$$

The angular limits of the passive joints are chosen by

$$\beta_{\min} = 30^\circ,\ \beta_{\max} = 150^\circ,\ \gamma_{\max} = 30^\circ.$$

Since the intersection of Eqs. (30a) and (30b) does not exist for the given angular limits, $\beta_{\max}$ is modified to $\beta'_{\max} = 153^\circ$ in Eq. (30a). The resulting intersection is obtained as shown in Fig. 7. In this design, the minimum l_{z1} (Q_1) is selected for larger force transmission capability at the end-effector. Table 1 shows the optimal design result. The kinematic parameters in the prototype are slightly different from the optimal design result.

The workspace of the prototype haptic device is shown in Fig. 8, where the following rotary actuator ranges from the mechanical interference are considered.

$$-155^\circ \le \theta_{1,1} \le 90^\circ,\ -90^\circ \le \theta_{2,1} \le 155^\circ$$

It has been demonstrated that the workspace of the haptic device with a redundant actuator is much larger than that without a redundant actuator ($\alpha = 0$).

Figure 9 shows the force transmission capabilities along the x-, y- and z-axes for the maximum actuator torque, $\tau_{i,\max} = 1.11$ [Nm]. Figure 10 plots the diagonal element of the Cartesian stiffness matrix in Eq. (21) for the joint stiffness, $k_i = 55.58$ [Nm/rad]. The averaged values of forces and stiffnesses are given by

$$f_x = 12.92,\ f_y = 9.77,\ f_z = 7.16\ [\text{N}],$$

$$k_{11} = 4.69,\ k_{22} = 2.37,\ k_{33} = 2.69\ \ [\text{N/mm}].$$

It should be noted that this device has good force reflection and stiffness along the x-axis.

As shown in Figs. 11 and 12, the 4-axis controller consists of Host PC with Simulink and Target PC with xPC Target from MathWorks. Figure 13 shows the prototype haptic device which was upgraded from the first prototype in [29]. Three DC servo motors and wire-driven gears (gear ratio=9.5:1) are used for 3-axis force reflection and joint angle sensing. The gravity force of the moving parts is compensated by the DC servo motors. One geared AC servo motor (gear ratio=45:1) is used for the position control of α.

Parameters	Optimal design	Prototype design
l_{p1}	159.90	159
l_{p2}	180.00	180
l_{z1}	162.67	162
l_{z2}	182.85	180

Table 1. Optimized design parameters.

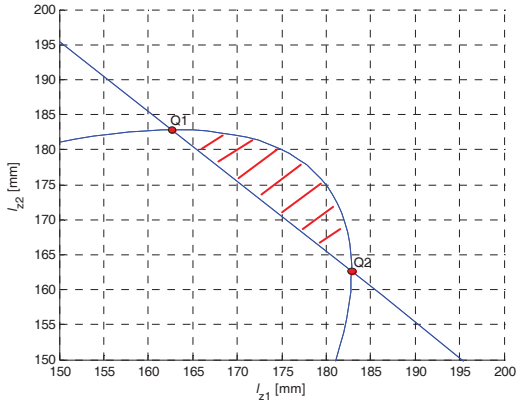

Figure 7. The intersection area of l_{z1} and l_{z2}.

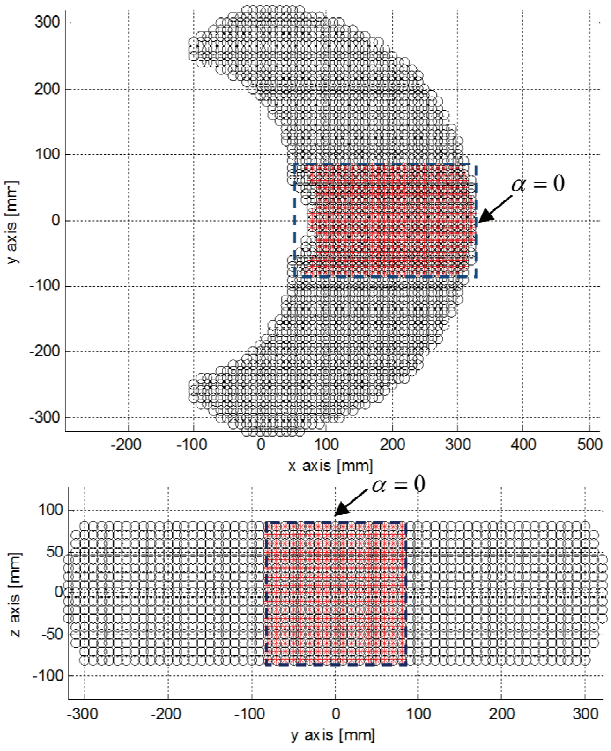

Figure 8. Workspace of the prototype haptic device.

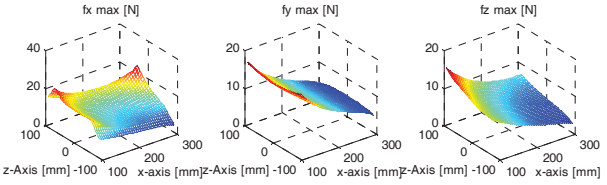

Figure 9. Mesh plot of force transmission capability on the $x'z$ plane.

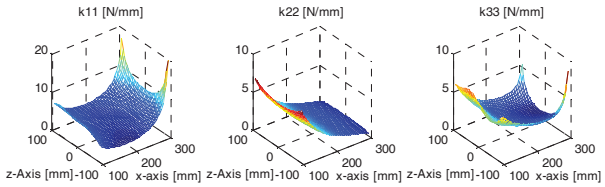

Figure 10. Mesh plot of Cartesian stiffness on the $x'z$ plane

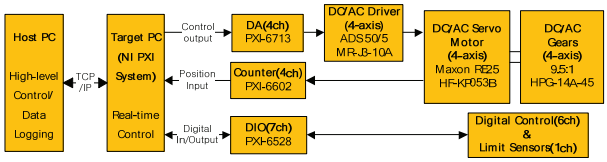

Figure 11. Block diagram of a PC-based real-time controller.

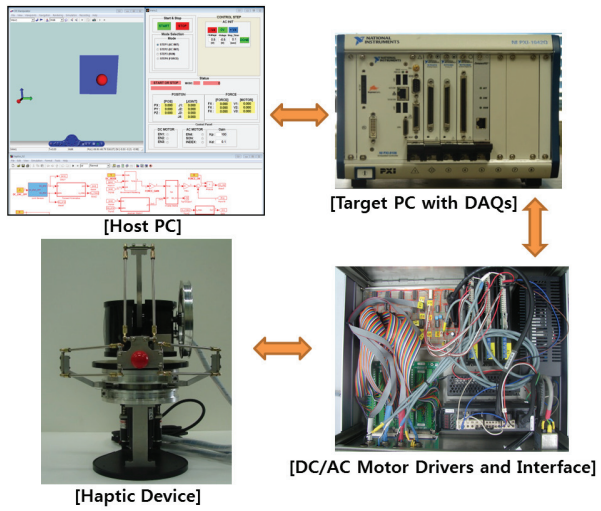

Figure 12. System configuration of a haptic device.

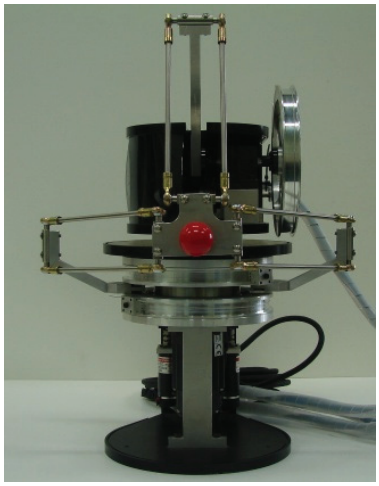

Figure 13. Prototype parallel haptic device.

Finally, the control experiment on the redundant actuator is performed. The handle of the haptic device is moved from $y=-100$ to $y=+100$ [mm] roughly by hand as shown in Fig. 14. The actuator angles are measured by corresponding DC motor encoders, the end-effector position is calculated through the forward position analysis and the redundant actuator's angle is commanded as $\alpha=\tan^{-1}(p_y/p_x)$ at every 1msec. It can be seen that the redundant actuator follows the operator's position very well.

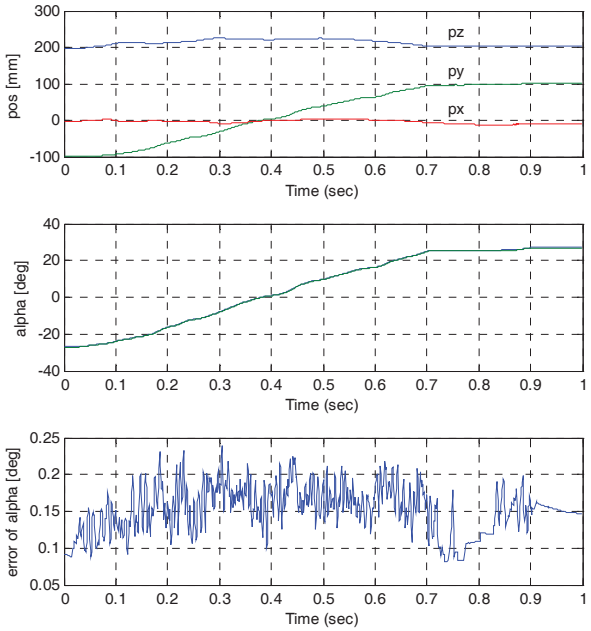

Figure 14. Control experiment on the redundant actuator when the moving platform moves along the y-axis.

6. Conclusion

In this paper, a Delta-type parallel manipulator with one redundant actuator is conceived for the 3-DOF positioning haptic device with a large workspace. The position, Jacobian and workspace analyses of the 3-DOF positioning parallel haptic device are presented. The optimal design method of finding minimum link lengths to satisfy the prescribed workspace is developed and applied to the prototype haptic device design. The prototype haptic device and 4-axis PC-based real-time controller using xPC target have been developed. Finally, it is demonstrated through analysis and experiment that by adding one redundant actuator to the third leg and using the simple control method of $\alpha=\tan^{-1}(p_y/p_x)$, the workspace can be increased significantly and good kinematic performance can be maintained over the whole workspace.

7. Acknowledgements

This work was supported by Kyungnam University Foundation Grant, 2009.

8. References

[1] Cavusoglu, M. C., Feygin D., Tendick, F. (2002), A Critical Study of the Mechanical and Electrical Properties of the PHANToM Haptic Interface and Improvements for High-Performance Control, The MIT Press Journals, Vol. 11, No. 6, pp. 555-568.

[2] Chen, E. (1999), Six Degree-of-Freedom Haptic System For Desktop Virtual Prototyping Applications, Proceedings of the International Workshop on Virtual Reality and Prototyping, Laval, France, pp. 97-106.

[3] Cohen A., Chen, E. (1999), Six Degree-of-Freedom Haptic System as a Desktop Virtual Prototyping Interface, Proceedings of the ASME Winter Annual Meeting, Dynamics Systems and Control, Nashville, Tennessee, Vol. 67, pp. 401-402.

[4] Sensable: http://www.sensable.com

[5] Ueberle, M., Buss, M. (2002), Design, Control, and Evaluation of a New 6 DOF Haptic Device, Proceedings of the IEEE International Conference on Intelligent Robots and Systems, Lausanne, Switzerland, pp. 2949-2954.

[6] Ueberle, M., Mock, N., Buss, M. (2004), ViSHaRD10, a Novel Hyper-Redundant Haptic Interface, Proceedings of the IEEE 12th International Symposium on Haptic Interfaces for Virtual Environment and Teleoperator Systems, Chicago, Illinois, USA, pp. 58- 65.

[7] Hayward, V. (1995), Toward a Seven Axis Haptic Interface, Proceedings of the IROS International Workshop on Intelligent Robots and Systems, Vol. 2, pp. 133-139.

[8] Hayward, V., Gregorio, P., Astley, O. R., Greenish, S., Doyon, M. (1997), Freedom-7: A High Fidelity Seven Axis Haptic Device With Application To Surgical Training, Proceedings of the ISER 6th International Symposium on Experimental Robotics, Vol. 5.

[9] Campion, G., Wang, Q., Hayward, V. (2005), The Pantograph Mk-II: A Haptic Instrument, Proc. IROS 2005, IEEE/RSJ Int. Conf. Intelligent Robots and Systems, pp. 723-728.

[10] Birglen, L., Gosselin, C., Pouliot, N., Monsarrat, B., Laliberte, T. (2002), SHaDe, A New 3-DoF Haptic Device, IEEE Transactions on Robotics and Automation, Vol. 18, pp. 166-175.

[11] Sirouspour, M. R., DiMaio, S. P., Salcudean, S. E., Abolmaesumi, P., Jones, C. (2000), Haptic Interface Control - Design Issues and Experiments with a Planar Device, Proceedings of the IEEE International Conference on Robotics & Automation.

[12] Stocco, L. J., Salcudean, S. E., Sassani, F. (2001), Optimal Kinematic Design of a Haptic Pen, IEEE/ASME Transactions on Mechatronics, Vol. 6, No. 3, pp. 210-220.

[13] Tsumaki, Y., Naruse, H., Nenchev, D. N., Uchiyama, M. (1998), Design of a Compact 6-DoF Haptic Interface, Proceedings of the IEEE International Conference on Robotics & Automation, pp. 2580-2585.

[14] Long, G. L., Collins, C. L. (1992), A Pantograph Linkage Parallel Platform Master Hand Controller for Force-Reflection, Proceedings of the IEEE International Conference on Robotics and Automation, Nice, France, pp. 390-395.

[15] Pierrot F., Reynaud C., FournierA. (1990), DELTA: A Simple and Efficient Parallel Robot. Robotica. Vol. 8, pp. 105-109.

[16] Grange S., Conti F., Helmer P., Rouiller P., Baur C. (2001), The Delta Haptic Device as a Nanomanipulator, SPIE Microrobotics and Microassembly III, Boston, MA.

[17] Yoon W. K., Seuhiro T., Tsumaki Y., Uchiyama M. (2004), Stiffness Analysis and Design of a Compact Modified Delta Parallel Mechanism,Robotica, Vol. 22, pp. 463-475.

[18] Force Dimension: http://www.forcedimension.com

[19] ZhuZ., Li J., Gan Z., Zhang H. (2005), Kinematic and Dynamic Modelling for Real-time Control of Tau Parallel Robot, Mechanism and Machine Theory, Vol. 40, pp. 1051-1067.

[20] Williams I., Hovland G., Brogardh T. (2006), Kinematic Error Calibration of the Gantry-Tau Parallel Manipulator, Proc. of the 2006 IEEE International Conference on Robotics and Automation, Orlando, Florida.

[21] Brodgardh T. (2007), Present and future robot control development – An industrial perspective, Annual Reviews in Control, Vol. 21, pp. 69-79.

[22] Martin J., Savall, J. (2005), Mechanism for Haptic Torque Feedback, Proceedings of the First Joint Eurohaptics Conference and Symposium on Haptic Interfaces for Virtual Environment and Teleoperator System.

[23] Kim H. S. (2010), Mechanism Design of Haptic Devices, In Zadeh M. H. editor. Advances in Haptics, InTech, pp. 283-297.

[24] Ebrahimi I., Carretero J. A., Boudreau R. (2007), 3-PRRR redundant planar parallel manipulator: Inverse displacement, workspace and singularity analyses. Mechanism and Machine Theory, Vol. 42, pp. 1007-1016.

[25] Mohamed M. G., Gosselin C. M. (2005), Design and Analysis of Kinematically Redundant Parallel Manipulators With Configurable Platforms, Vol. 21, No. 3, pp. 277-287.

[26] Salisbury, J. K., Craig, J. J. (1982), Articulated Hands: Force Control and Kinematics Issues, International Journal of Robotics Research, Vol. 1, No. 1, pp. 4-17.

[27] Kim, H. S., Choi, Y. J. (2001), Forward/Inverse Force Transmission Capability Analyses of Fully Parallel Manipulators, IEEE Transaction on Robotics and Automation, Vol. 17, No. 4, pp. 526-530.
[28] Tsai, L. W. (1999), Robot Analysis: The Mechanics of Serial and Parallel Manipulators, John Wiley & Sons, Canada, pp. 134-142.
[29] Kim, H. S. (2007), Design of a Novel 3-DOF Parallel-type Haptic Device with Redundant Actuation, International Conference on Control, Automation and Systems, Seoul, Korea.